

## Supporting Information

# Elucidating the Trade-off between Membrane Wetting Resistance and Water Vapor Flux in Membrane Distillation

Chenxi Li<sup>1</sup>, Xuesong Li<sup>2,\*</sup>, Xuewei Du<sup>3</sup>, Ying Zhang<sup>1</sup>, Wei Wang<sup>4</sup>, Tiezheng Tong<sup>3</sup>,  
Arun Kumar Kota<sup>4</sup>, and Jongho Lee<sup>1,\*</sup>

<sup>1</sup> *Department of Civil Engineering, University of British Columbia, Vancouver,  
British Columbia, Canada*

<sup>2</sup> *State Key Laboratory of Pollution Control and Resource Reuse, Shanghai Institute of Pollution Control and Ecological Security, School of Environmental Science and Engineering, Tongji University, 1239 Siping Road, Shanghai 200092, China*

<sup>3</sup> *Department of Civil and Environmental Engineering, Colorado State University, Fort Collins, Colorado, United States*

<sup>4</sup> *Department of Mechanical and Aerospace Engineering, North Carolina State University, Raleigh, North Carolina, United States*

\* Corresponding authors:

Xuesong Li, Email: [xuesong\\_li@tongji.edu.cn](mailto:xuesong_li@tongji.edu.cn), Phone: 86-21-65975669

Jongho Lee, Email: [jongho.lee@civil.ubc.ca](mailto:jongho.lee@civil.ubc.ca), Phone: (604) 822-4694

Number of Pages: 12

Number of Tables: 2

Number of Figures: 5

**Table S1.** Summary of the water flux data of the membrane before ( $J_{\text{before}}$ ) and after ( $J_{\text{after}}$ ) the surface modification with low surface energy materials in the literature and the water flux ratios ( $J_{\text{after}}/J_{\text{before}}$ ), as well as the corresponding membrane characteristic changes calculated from the data in the literature.

Number	Water Flux Before Modification ( $J_{\text{before}}$ ) [L m <sup>-2</sup> h <sup>-1</sup> ]	Water Flux After Modification ( $J_{\text{after}}$ ) [L m <sup>-2</sup> h <sup>-1</sup> ]	Ratio of Water Flux ( $J_{\text{after}}/J_{\text{before}}$ )	Relative Pore Size Change After Modification	Relative Porosity Change After Modification	Relative Thickness Change After modification	Reference
<b>PVDF-HFP based membranes</b>							
1	~23.5	~12.5	0.532	n.a.	n.a.	n.a.	Lee et al., 2016 <sup>1</sup>
2	31.4	13.3	0.424	n.a.	n.a.	n.a.	Huang et al., 2017 <sup>2</sup>
3	21	~19	0.905	n.a.	2.5 % ↓	3 % ↓	An et al., 2018 <sup>3</sup>
4	~11	~9	0.818	n.a.	n.a.	n.a.	Lu et al., 2018 <sup>4</sup>
<b>PVDF based membranes</b>							
5	23.5	13.6	0.579	n.a.	n.a.	n.a.	Boo et al., 2016 <sup>5</sup>
6	30	25.2	0.840	n.a.	n.a.	n.a.	Lu et al., 2017 <sup>6</sup>
7	13.17	11.22	0.852	55% ↓	5 % ↓	7 % ↑	Woo et al., 2018 <sup>7</sup>
8	~10.7	~9.7	0.907	3.5 % ↑	n.a.	0.5 % ↑	Zheng et al., 2018 <sup>8</sup>
9	24.9	18.3	0.735	0.3 % ↓	1.5 % ↓	n.a.	Lu et al., 2018 <sup>9</sup>
10	~5.7	~4.7	0.825	24 % ↓	1 % ↓	2 % ↑	Wang et al., 2018 <sup>10</sup>
11	30.9	23.4	0.757	n.a.	n.a.	n.a.	Du et al., 2018 <sup>11</sup>
12	18	14	0.778	n.a.	n.a.	n.a.	Karanikola et al., 2018 <sup>12</sup>
13	~29.1	~19.3	0.66	1 % ↑	n.a.	n.a.	Wang et al., 2019 <sup>13</sup>
14	32	27.78	0.868	n.a.	6 % ↓	n.a.	Chen et al., 2020 <sup>14</sup>

n.a. : not available

↑ : increase

↓ : decrease

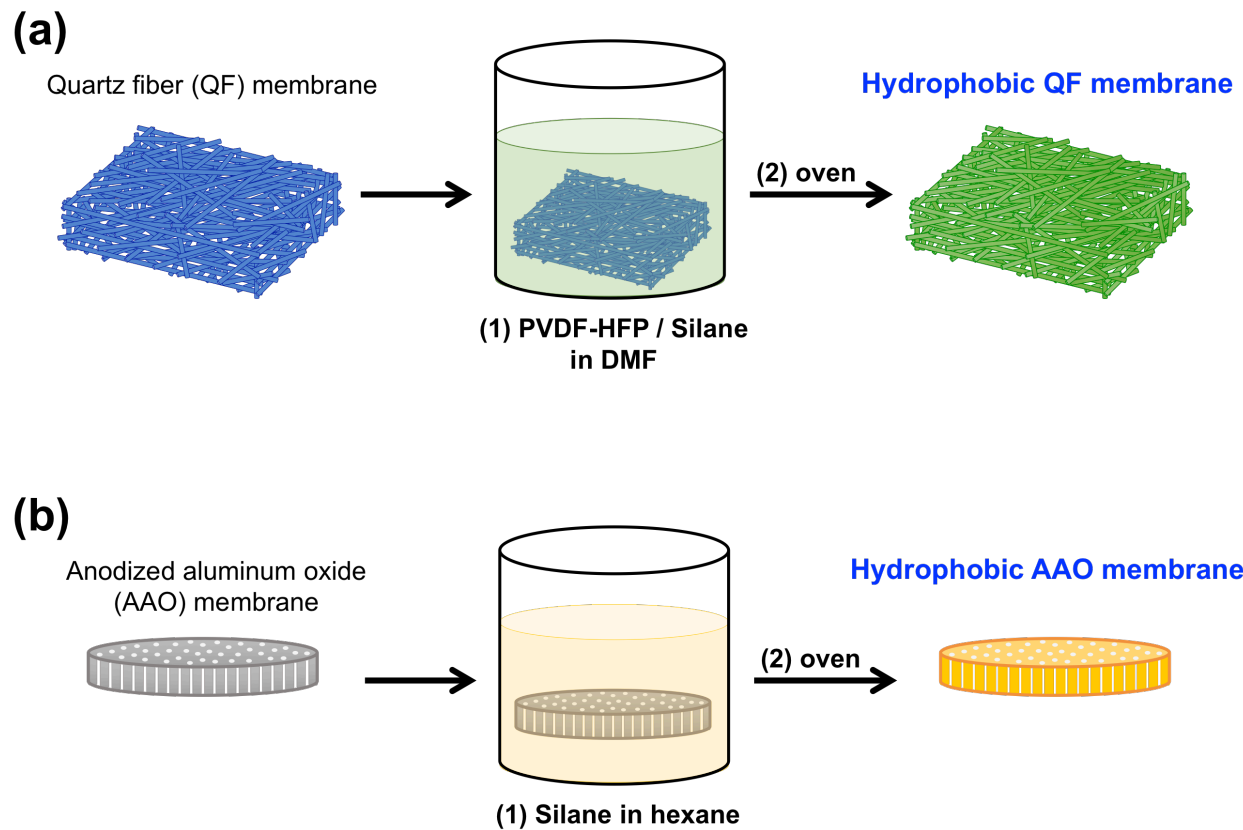


**Figure S1.** Schematic illustration of hydrophobic modification processes of (a) QF membranes and (b) AAO membranes.

**Section 1. Estimation of capacitance using EIS.** When immersed in the electrolyte solution, the unwetted hydrophobic membrane will keep air trapped in membrane pores and make two liquids separated. In this scenario, with the negligibly small impedance across the electrolyte (1 M NaCl solution), the membrane can be modeled as a parallel circuit of a resistor and a capacitor in the EIS.<sup>15, 16</sup> The impedance of the membrane,  $Z$ , can be expressed as:

$$Z = \frac{1}{\frac{1}{R} + j\omega C} \quad (\text{S1.})$$

where  $R$  is the resistance of air-filled hydrophobic membrane ( $\Omega$ ),  $j$  is the imaginary unit,  $\omega$  is angular frequency (rad/s) and  $\omega = 2\pi f$ , where  $f$  is the frequency of the applied potential (Hz), and  $C$  is the capacitance ( $F$ ). The magnitude of the impedance,  $|Z|$ , is then calculated as:

$$|Z| = \frac{1}{\sqrt{\frac{1}{R^2} + \omega^2 C^2}} \quad (\text{S2.})$$

When tested with a high frequency ( $\omega \gg R^{-1}C^{-1}$ ), the capacitive reactance ( $\omega^{-1}C^{-1}$ ) becomes the dominant part of the impedance and thus  $|Z|$  can be approximated to:

$$|Z| \cong \frac{1}{\omega C} = \frac{1}{2\pi f C} \quad (\text{S3.})$$

Eq. (S3) can then be rewritten as:

$$\ln|Z| = -\ln f - \ln(2\pi C) \quad (\text{S4.})$$

Based on Eq. (S4), the plot of  $\ln|Z|$  versus  $\ln f$  shows a straight line with slope of approximately  $-1$  in the high-frequency zone (See Figure S4 as an example). We determined the capacitance ( $C$ ) using the impedance measured at the highest testing frequency,  $10^6$  Hz.

**Section 2. Membrane structure characterizations.** The membrane thickness was determined with an electronic micrometer. The maximum and mean pore sizes of the modified membranes were measured by capillary flow porometry (3H-2000PB, Beishide Instrument). All samples were firstly applied with compressed nitrogen gas to determine the gas permeability. Subsequently the dry membrane samples were completely wetted by a low-surface-tension liquid (Porefil,  $\gamma=16 \text{ mN}\cdot\text{m}^{-1}$ ) and tested under the same condition.

Gravimetric method was used to determine the membrane porosity by measuring the weight of modified QF membrane and pristine QF membranes. All membranes were cut into circular samples (diameter is 22.0 cm) with a punch cutter. The porosity of the membranes ( $\varepsilon_P$ ) can be calculated using the following equation:

$$\varepsilon_P = 1 - \frac{\frac{W_m - W_{QF}}{D_{PVDF-HFP}} + \frac{W_{QF}}{D_{Quartz}}}{A \cdot l} \quad (\text{S5.})$$

where  $W_m$  and  $W_{QF}$  are the weights of the modified membranes and pristine QF membrane, respectively;  $D_{PVDF-HFP}$  ( $1.78 \text{ g}\cdot\text{cm}^{-3}$ ) and  $D_{Quartz}$  ( $2.65 \text{ g}\cdot\text{cm}^{-3}$ ) are densities of PVDF-HFP and quartz fiber, respectively;  $A$  refers to the surface area of the membrane sample and  $l$  is the membrane thickness.

The liquid entry pressure (LEP) was investigated by using a homemade transparent dead-end membrane cell. In brief, a dry membrane sample was secured in the membrane cell and then the cell was filled with 25 mL distilled water. A vacuum pressure was then progressively applied on the permeate side until the first sign of water droplet coming out from the back surface of the membrane, when the pressure was recorded as the LEP of the membrane sample. At least triplicate measurements with different membranes were tested for the calculation of the averaged LEP.

**Section 3. Measurement of water vapor flux and salt rejection in DCMD experiments.** The weight change in the permeate was monitored by a digital balance (Symmetry 4202E PT, Cole-Parmer) with an accuracy of  $\pm 0.01$  g and the weight data was collected by WinWedge software (TALtech, PA) to calculate the real-time water flux,  $J_w$  ( $\text{L}\cdot\text{m}^{-2}\cdot\text{h}^{-1}$ ), using the following equation:

$$J_w = \frac{\Delta m_P}{\rho A_m \Delta t} \times 1000 \quad (\text{S6.})$$

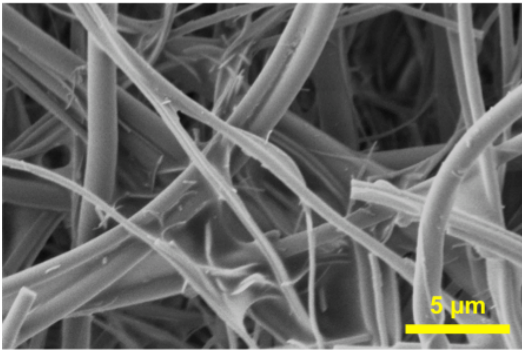
where  $\Delta m_P$  (kg) is the mass change of the permeate solution during the time period of  $\Delta t$ ,  $\rho$  is the water density ( $\text{kg}\cdot\text{m}^{-3}$ ),  $A_m$  is the effective membrane area ( $\text{m}^2$ ), and  $\Delta t$  is the time interval (h).

The conductivity of the permeate solution was monitored in real-time by a conductivity meter (Oakton CON 2700, Oakton Instruments, Vernon Hills, IL) with a built-in software and the conductivity meter has a measurement accuracy of  $\pm 0.1$   $\mu\text{S cm}^{-1}$ . The salt (NaCl) rejection,  $R$ , was calculated by using the following equation:

$$R = 1 - \frac{\Delta(V_P C_{SP}) / J_w A_m \Delta t}{C_{SF}} \quad (\text{S7.})$$

where  $V_P$  is the total permeate volume (L).  $C_{SF}$  and  $C_{SP}$  are the salt concentrations in the feed and permeate solutions, respectively.  $\Delta(V_P C_{SP})$  indicates the total mass of salt that passed through the membrane during the time period of  $\Delta t$ .

**(a)**



**(b)**

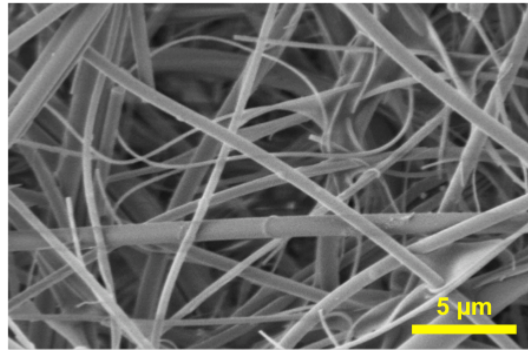


**Figure S2.** SEM micrographs of the morphologies of (a) FAS-3 QF membrane and (b) FAS-9 QF membrane.

**Table S2.** Characteristics of modified QF membranes

Membranes	Thickness (mm)	Porosity (%)	Mean pore size ( $\mu\text{m}$ )	Max. pore size ( $\mu\text{m}$ )	Liquid entry pressure (LEP) (kPa)
QF-AS	$0.568 \pm 0.007$	$90.9 \pm 0.2$	$4.21 \pm 0.30$	$5.88 \pm 0.04$	$28.5 \pm 0.5$
QF-FAS-3	$0.573 \pm 0.005$	$90.8 \pm 0.4$	$4.38 \pm 0.18$	$5.89 \pm 0.17$	$32.5 \pm 0.5$
QF-FAS-9	$0.576 \pm 0.004$	$91.0 \pm 0.2$	$4.27 \pm 0.16$	$6.00 \pm 0.01$	$33.8 \pm 1.0$
QF-FAS-17	$0.570 \pm 0.003$	$90.8 \pm 0.2$	$4.19 \pm 0.16$	$5.83 \pm 0.21$	$39.0 \pm 0.8$

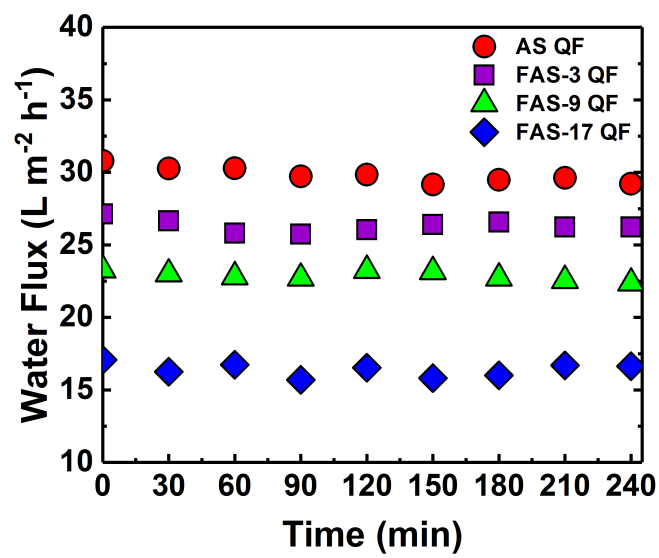


**Figure S3.** Water vapor fluxes of the AS QF (circle symbols), FAS-3 QF (square symbols), FAS-9 QF (triangle symbols), and FAS-17 QF (diamond symbols) membranes in DCMD tests using 0.5 M NaCl at 60 °C as the feed solution and distilled water at 20 °C as the permeate solution. All membranes showed a salt rejection higher than 99.5% over the entire tests.

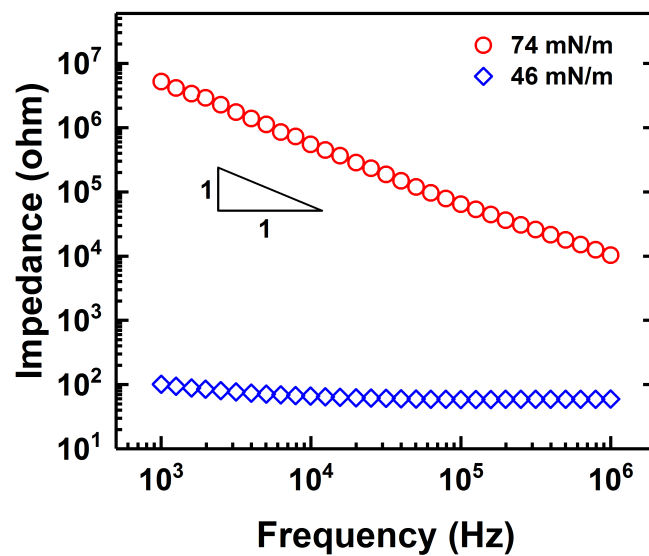


**Figure S4.** Impedance spectra of AS QF membrane obtained by using 1 M NaCl solution ( $\gamma = 74 \text{ mN/m}$ , circle symbols) and 1M NaCl solution with 0.05 mM SDS ( $\gamma = 46 \text{ mN/m}$ , diamond symbols) as the electrolyte solution.

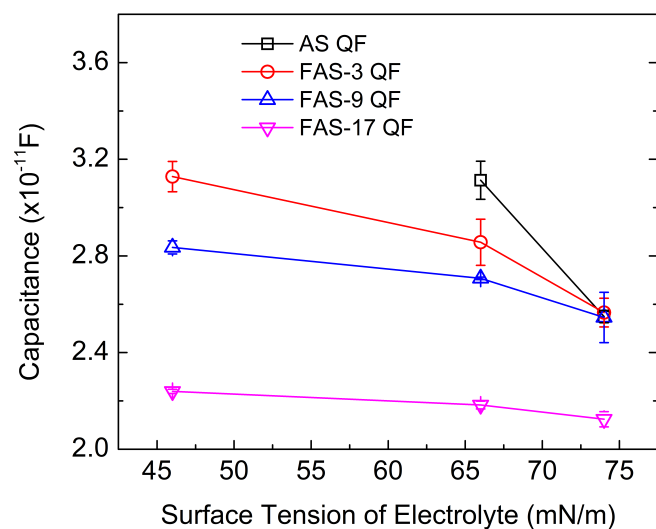


**Figure S5.** Estimated capacitances of the modified QF membranes based on the impedance measurements using 1 M NaCl solution with different surface tensions (SDS added) as the electrolyte solution. Error bars represent standard deviations from three different membrane samples modified with each different silane.

## REFERENCES

1. Lee, J.; Boo, C.; Ryu, W. H.; Taylor, A. D.; Elimelech, M., Development of Omniphobic Desalination Membranes Using a Charged Electrospun Nanofiber Scaffold. *ACS Appl Mater Interfaces* **2016**, *8*, (17), 11154-11161.
2. Huang, Y. X.; Wang, Z.; Jin, J.; Lin, S., Novel Janus Membrane for Membrane Distillation with Simultaneous Fouling and Wetting Resistance. *Environ Sci Technol* **2017**, *51*, (22), 13304-13310.
3. An, X.; Liu, Z.; Hu, Y., Amphiphobic surface modification of electrospun nanofibrous membranes for anti-wetting performance in membrane distillation. *Desalination* **2018**, *432*, 23-31.
4. Lu, C.; Su, C.; Cao, H.; Ma, X.; Duan, F.; Chang, J.; Li, Y., F-POSS based Omniphobic Membrane for Robust Membrane Distillation. *Materials Letters* **2018**, *228*, 85-88.
5. Boo, C.; Lee, J.; Elimelech, M., Omniphobic Polyvinylidene Fluoride (PVDF) Membrane for Desalination of Shale Gas Produced Water by Membrane Distillation. *Environ. Sci. Technol.* **2016**, *50*, (22), 12275-12282.
6. Lu, X.; Peng, Y.; Qiu, H.; Liu, X.; Ge, L., Anti-fouling membranes by manipulating surface wettability and their anti-fouling mechanism. *Desalination* **2017**, *413*, 127-135.
7. Woo, Y. C.; Kim, Y.; Yao, M.; Tijing, L. D.; Choi, J. S.; Lee, S.; Kim, S. H.; Shon, H. K., Hierarchical Composite Membranes with Robust Omniphobic Surface Using Layer-By-Layer Assembly Technique. *Environ. Sci. Technol.* **2018**, *52*, (4), 2186-2196.
8. Zheng, R.; Chen, Y.; Wang, J.; Song, J.; Li, X.-M.; He, T., Preparation of omniphobic PVDF membrane with hierarchical structure for treating saline oily wastewater using direct contact membrane distillation. *J. Membr. Sci.* **2018**, *555*, 197-205.
9. Lu, K. J.; Zuo, J.; Chang, J.; Kuan, H. N.; Chung, T.-S., Omniphobic Hollow-Fiber Membranes for Vacuum Membrane Distillation. *Environ. Sci. Technol.* **2018**, *52*, (7), 4472-4480.
10. Wang, M.; Liu, G.; Yu, H.; Lee, S.-H.; Wang, L.; Zheng, J.; Wang, T.; Yun, Y.; Lee, J. K., ZnO Nanorod Array Modified PVDF Membrane with Superhydrophobic Surface for Vacuum Membrane Distillation Application. *ACS Appl. Mater. Interfaces* **2018**, *10*, (16), 13452-13461.
11. Du, X.; Zhang, Z.; Carlson, K. H.; Lee, J.; Tong, T., Membrane fouling and reusability in membrane distillation of shale oil and gas produced water: Effects of membrane surface wettability. *J. Membr. Sci.* **2018**, *567*, 199-208.
12. Karanikola, V.; Boo, C.; Rolf, J.; Elimelech, M., Engineered Slippery Surface to Mitigate Gypsum Scaling in Membrane Distillation for Treatment of Hypersaline Industrial Wastewaters. *Environ. Sci. Technol.* **2018**, *52*, (24), 14362-14370.
13. Wang, W.; Du, X.; Vahabi, H.; Zhao, S.; Yin, Y.; Kota, A. K.; Tong, T., Trade-off in membrane distillation with monolithic omniphobic membranes. *Nat Commun* **2019**, *10*, (1), 3220.
14. Chen, Y.; Lu, K. J.; Chung, T.-S., An omniphobic slippery membrane with simultaneous anti-wetting and anti-scaling properties for robust membrane distillation. *J. Membr. Sci.* **2020**, *595*, 117572.
15. Chen, Y.; Wang, Z.; Jennings, G. K.; Lin, S., Probing Pore Wetting in Membrane Distillation Using Impedance: Early Detection and Mechanism of Surfactant-Induced Wetting. *Environ. Sci. Technol. Lett.* **2017**, *4*, (11), 505-510.
16. Wang, Z.; Chen, Y.; Sun, X.; Duddu, R.; Lin, S., Mechanism of pore wetting in membrane distillation with alcohol vs. surfactant. *J. Membr. Sci.* **2018**, *559*, 183-195.